JOURNAL OF MATERIALS SCIENCE 28 (1993) 4910–4917

Depth measurement of short cracks with an acoustic microscope

D. KNAUSS, D. D. BENNINK, T. ZHAI, G. A. D. BRIGGS, J. W. MARTIN
Department of Metallurgy and Science of Materials, University of Oxford, Oxford OX13PH, UK

The depth of short cracks (70–200 μm surface length) has been measured with an acoustic microscope by utilizing the nondestructive time-of-flight diffraction technique (TOFD). The depth measurements were first carried out in the transparent polymer polystyrene, thus allowing a comparison between the acoustical values and direct optical measurements: the agreement in the results was better than 95%. The depth of a 70 μm long crack in an aluminium alloy was then measured, demonstrating the application of the technique to metals.

1. Introduction

The growth behaviour of short cracks has been studied using both light microscopy and scanning electron microscopy. Perhaps the most common method used to examine the behaviour of short cracks is a replica technique based on taking several plastic replicas at various stages during a fatigue test and examining the replicas later with a light or electron microscope to determine the growth rate [1]. However, this method only gives information about the crack growth at the surface of the specimen, while the depth of the crack must be determined indirectly by assuming the crack has a given shape. The use of acoustic waves offers the possibility of measuring the depth of cracks directly, because the acoustic waves can penetrate into the specimen. One technique for determining the depth of cracks with acoustic waves is called the time-of-flight diffraction (TOFD) technique [2]. The TOFD technique is based on timing measurements made on the signals diffracted from the crack tip. A transducer emits a short acoustic pulse into the material which is scattered by the crack. The crack face acts like a mirror for the ultrasound and reflects part of the pulse energy, while another part is diffracted by the crack tip. This diffracted signal is of particular interest because, when it returns to the emitting transducer or to a separate receiving transducer, it can be used to determine the crack depth. The depth is calculated from the propagation time of the diffracted pulse taking into account the velocity of acoustic waves in the material. However, current applications of TOFD, for example *in situ* measurements of fatigue crack growth and in-service inspections of nuclear vessels, have been developed for larger cracks of the order of millimetres in depth [2].

In this work short cracks were studied, of the order of micrometres in depth, using the scanning acoustic microscope (SAM) at Oxford [3]. The Oxford SAM is an acoustic microscope with a point focus lens which can be operated in two different modes: a single frequency/CW mode, used to locate cracks and measure their surface length, and a pulse mode, used for TOFD. In the pulse mode the lens emits short pulses at a centre frequency of 220 MHz and a pulse length of about 5 ns. The use of such short pulses allows the measurement of the depth of a crack down to a minimum depth of about 10 μm in aluminium, for example. The aim of this work was to demonstrate that it is possible to measure the depth of short cracks with the SAM utilizing the TOFD technique. In order to verify this, the depth of short cracks in the transparent material polystyrene was determined. This work was an extension of earlier experiments on the transparent material perspex [4]. A transparent material was used because the acoustic measurements could then be compared with direct optical measurements. Also, polystyrene has the advantage that the cracks are usually straight along the surface with a simple geometry into the specimen, unlike cracks in metals which typically have a considerably more complicated shape.

In the following paragraphs we will briefly describe the TOFD technique and how the information concerning the crack geometry can be extracted from the experimental data. More details about TOFD and acoustic microscopy can be found elsewhere, for example [2, 5–6] and [7–10], respectively. Furthermore, we will then present the depth measurements for two cracks in polystyrene, and also for one crack in an aluminium alloy in order to demonstrate the application of this technique to metals.

2. Time-of-flight-diffraction technique (TOFD)

In the conventional TOFD technique a transmitter fires an ultrasonic pulse into the material and the diffracted signals are detected with a separate receiver. In the SAM the point focus lens acts as both the transmitter and the receiver. The first step of a TOFD measurement for the SAM is to locate the crack using the single frequency/CW mode of the microscope. The lens is then moved in 512 equally spaced steps unidirectionally across the specimen surface perpendicu-

0022–2461

lar to the trace of the crack (Fig. 1a) with the SAM switched to the pulse mode. At each point the lens emits a pulse into the specimen and receives the backscattered acoustic signal. This acoustic signal is converted into a voltage signal and displayed on a sampling oscilloscope. The signal is sampled at 512 equally spaced time points and the sampled values are transferred to a computer for processing and storage. After the 512 point scan across the crack is completed, the stored 512 lines, each of 512 sampling points, are displayed on a frame store with the voltage sample values converted into 256 grey levels (Fig. 1b). This display is referred to as an $s(t, y)$ image (scanning, time, y position image), while a single frequency mode image is referred to as an acoustic micrograph. Each $s(t, y)$ image consists of 512×512 image points with the horizontal axis representing time and the vertical axis representing the lens position .

Various signals can occur in an $s(t, y)$ image when the lens is scanned across a surface-breaking crack in a specimen. These signals are represented in Fig. 2 by ray diagrams and in Fig. 3 as a schematic $s(t, y)$ image. The signals are as follows.

(a) Specular reflection; part of the incident pulse is reflected directly by the specimen surface. The transit time of the specular reflection is independent of the lens position (if the lens moves parallel to the surface) and therefore its time position in an $s(t, y)$ image is constant (the first vertical line in Fig. 3).

(b) Surface-wave transmission; a surface wave, generated and received by a ray at the critical angle, is transmitted along the surface. The length of the path along the surface, and therefore the transit time, depends on the defocus of the lens but is not affected by the presence of the crack (defocus is the distance the lens is moved towards the specimen relative to focusing on the surface). Thus its time position in an $s(t, y)$ image is also constant (the second vertical line in Fig. 3). In a relatively low-stiffness material, such as polystyrene, the propagation along the surface is as a lateral longitudinal wave (or surface skimming compression wave) [11]; in high-stiffness materials, such as aluminium, the propagation along the surface is as a Rayleigh wave [12].

(c) Surface-wave reflection; a surface wave, as in (b), propagates along the surface and is reflected by the mouth of the crack back to the lens. There are actually two surface-wave reflections, because the surface wave

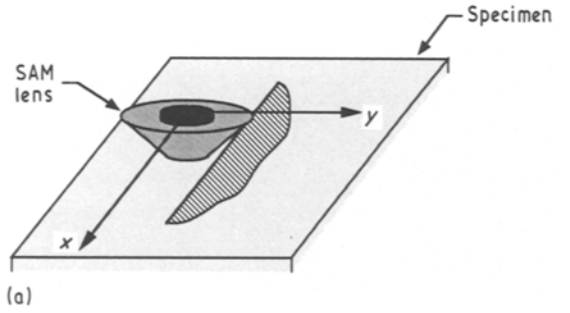

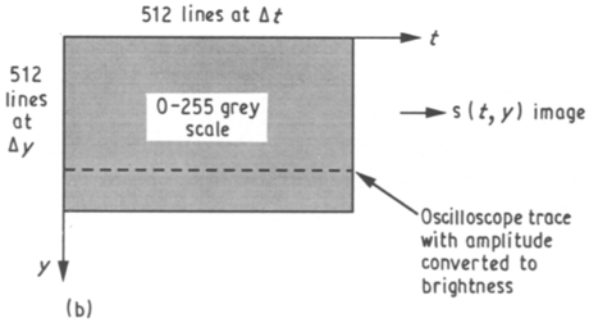

Figure 1 Generation of an $s(t, y)$ image (a) the lens of the acoustic microscope is moved in 512 steps across the crack in the y direction, (b) the grey scale $s(t, y)$ image (schematic).

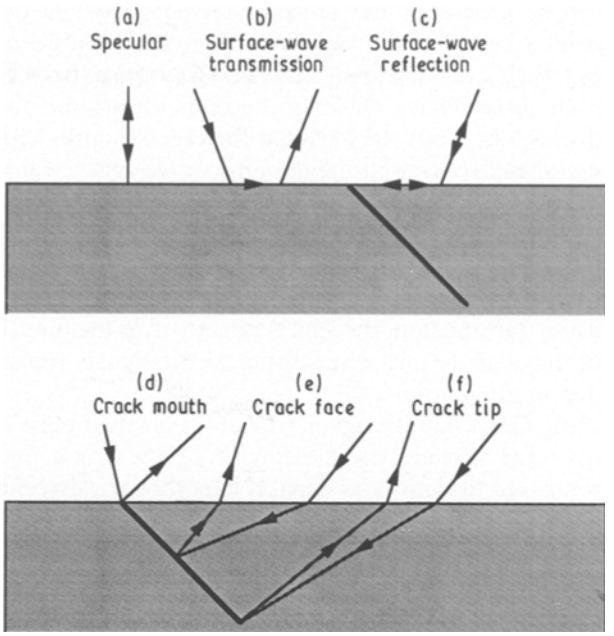

Figure 2 Ray diagrams of the reflected and diffracted signals from a specimen containing an oblique surface-breaking crack.

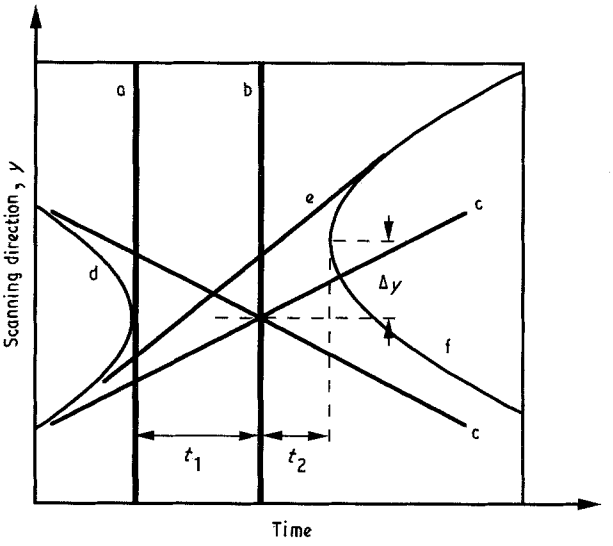

Figure 3 Schematic $s(t, y)$ image with the signals indicated in Fig. 2. The depth, d, of the crack can be determined from $\Delta t = t_1 + t_2$ and $d = (c\Delta t)/2$; c = velocity of sound in the material.

can be generated and reflected on both sides of the crack (there are also two surface-wave transmissions but they are indistinguishable). The transit time of each surface-wave reflection depends linearly on the distance between the lens and the crack mouth, with one signal arriving earlier than the surface-wave transmission, and one later [7]. This results in a crossing pattern in the $s(t, y)$ image (as shown in Fig. 3) and at the crossing point, where the two surface-wave reflections have the same transit time as that of the surface-wave transmission, the lens is directly over the mouth of the crack [3]. At large distances the signals vanish due to attenuation.

(d) Crack-mouth signal; part of the incident pulse is scattered directly by the mouth of the crack and returns to the lens. The signal is hyperbolic in shape in an $s(t, y)$ image and occurs before the specular signal, except when the lens is directly over the crack mouth and they coincide [13].

(e) Crack-face reflection; a ray propagates into the material, is reflected by the crack's face and returns to the lens. The crack face acts like a mirror and the ray path is determined by applying Snell's law to the reflection. In the $s(t, y)$ image the signal appears as a straight line with a slope depending on the inclination of the crack.

(f) Crack-tip signal; a ray propagates into the material, is diffracted by the crack tip and returns to the lens. The signal is approximately hyperbolic in shape in an $s(t, y)$ image and always occurs after the specular signal. The transit time of the signal is at a minimum when the lens is directly over the crack tip.

Signals a–d are independent of the crack geometry, while signal e contains information about the inclination of the crack, and signal f about the crack depth. Also, both Signals a and b will occur either with or without the presence of a crack.

Referring to Fig. 3, for a crack oriented perpendicular to the specimen surface, the vertex of the hyperbola-shaped tip-diffracted signal is at the same y position as the surface-wave reflection crossing point. However, if the crack is inclined, as assumed for Fig. 3, then the vertex is shifted in the y direction away from being directly below the crossing point and line e should appear. The angle β between the surface and the crack can be calculated from the slope $m = \delta y/\delta t$ of line e as $\beta = \arcsin(1/2\, c/m)$, where c is the wave velocity, or determined from the shift, Δy, in the vertex of the tip-diffracted signal as $\beta = \arctan(d/\Delta y)$, where d is the crack depth. The time distance, Δt, between the specular reflection and the tip-diffracted signal vertex, coupled with the knowledge of the linear elastic-wave speed, c, in the specimen, serves to determine the depth of the crack as

$$d = \frac{1}{2}(c\Delta t) \qquad (1)$$

However, because the specular reflection signal is very broad (see Fig. 4a), it is difficult to measure the time distance, Δt, directly. A more convenient method for evaluating Δt is to first measure the time distance, t_2, between the crossing point of the surface-wave reflection and the vertex of the tip-diffracted signal, because

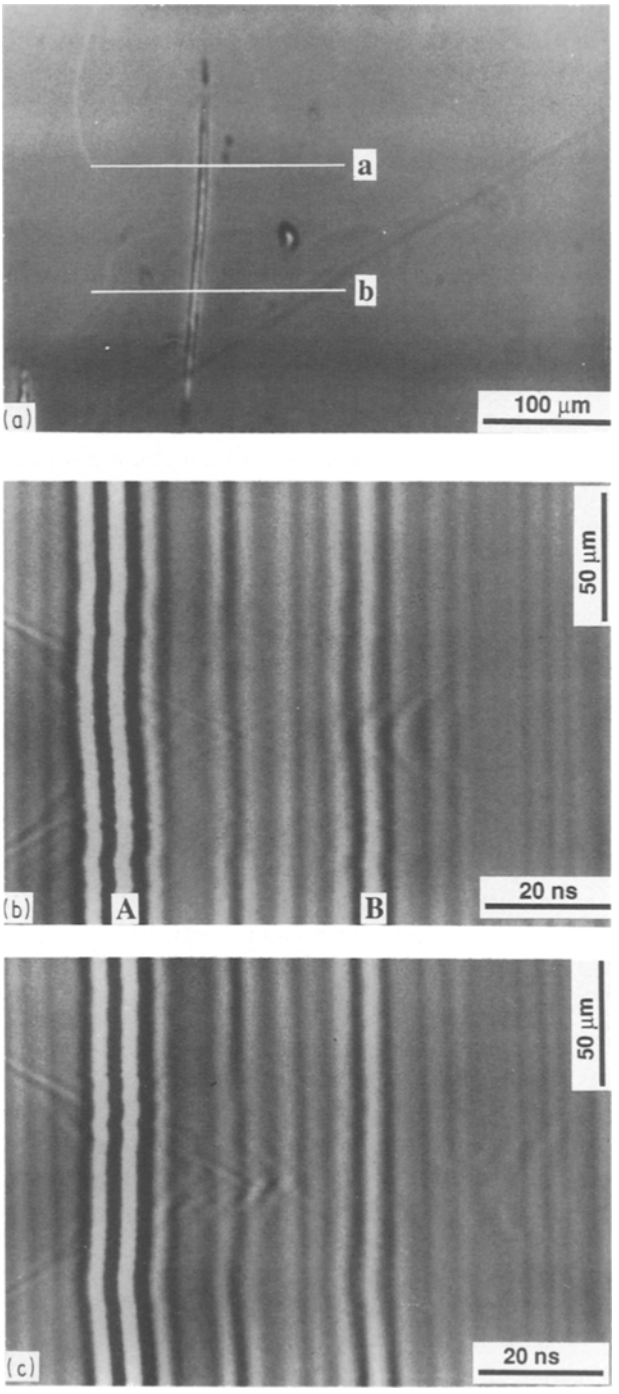

Figure 4 (a) Acoustic micrograph, $\Delta z = 0$ μm and $\nu = 350$ MHz, of crack 1 in polystyrene with scan positions a and b marked. (b) The $s(t, y)$ image at position a; $\Delta z = -60$ μm. (c) The $s(t, y)$ image at position b; $\Delta z = -60$ μm. For both (b) and (c) the time range in the horizontal direction is 100 ns and the scan range in the vertical direction is 170 μm.

the surface-wave crossing point is considerably more well defined. Then Δt is found from $\Delta t = t_1 + t_2$ with t_1 the time difference between the specular reflection and the surface-wave crossing point, which is calculated from

$$t_1 = \frac{2\Delta z}{c_w}[1 - (1 - n^2)^{1/2}] \qquad (2)$$

In Equation 2, Δz is the defocus value of the lens and n is the ratio c_w/c_o, with c_w the wave speed in water and c_o the surface wave velocity in the material [11, 12].

3. Results

Polystyrene is a transparent, brittle polymer with a density close to water ($\rho = 1.08\ g\,cm^{-2}$). The acoustic-wave velocities in polystyrene are: longitudinal $c_L = 2.35\ \mu m\,ns^{-1}$, shear $c_S = 1.12\ \mu m\,ns^{-1}$ and Rayleigh $c_R = 1.048\ \mu m\,ns^{-1}$. The cracks were produced by a deep indent in the middle of a 0.7 mm thick polystyrene slide which resulted in a long through-thickness crack with wedge-shaped ends. In the region of each end of this long crack, short cracks of the order of 80–300 μm in length occurred which were suitable for the depth measurements.

One major obstacle to determining crack depths using the tip-diffracted signal is the very small amplitude of this signal, resulting in part because the diffracted energy is spread over a large range of angles. Thus signal averaging is necessary in order to enhance the signal-to-noise ratio, i.e. repeating the time measurement at each scanning location several times [2].

Fig. 4a is an acoustic micrograph showing a 200 μm long crack in polystyrene (crack 1), taken with the SAM in the single frequency mode at 350 MHz and zero defocus. The two horizontal white lines in the image indicate the scanning positions (a and b) used for the TOFD measurements. The $s(t, y)$ images obtained at positions a and b are given in Fig. 4b and c, respectively, each at a defocus $\Delta z = -60\ \mu m$. The first strong set of vertical stripes on the left of the $s(t, y)$ image is the specular reflection, A, while the next vertical stripe system in strength further to the right is an echo of this signal, B. This echo is a result of an impedance mismatch between the connecting coaxial cable and both the lens and the receiver. The weaker set of vertical stripes appearing between the specular signal and its echo is the surface-wave transmission, verified by the crossing point of the surface-wave reflection signals. The other weaker sets of vertical lines which appear are caused by a background subtraction (used to extract the signal of interest out of a larger fixed background signal). Beyond the specular echo is the hyperbola-shaped crack tip-diffracted signal, and the depth of the crack can be calculated from the location of its vertex using Equations 1 and 2. For scanning positions a and b the depths thus obtained were 52 and 70 μm, respectively. In the $s(t, y)$ image in Fig. 4b, a shift Δy is not measurable and it can be concluded that the crack is oriented perpendicular to the surface at location a. From the $s(t, y)$ image in Fig. 4c, however, a shift Δy of 5 μm was measured so that at location b the crack is inclined to the surface at an angle 86°. Although no reflection from the crack face could be observed in either $s(t, y)$ image, this is consistent with the high inclination angle of the crack at both locations.

Fig. 5 shows schematically the shape of crack 1, and a comparison between the acoustic and direct optical measurements is given in Table I. The optical depth determination was carried out with a light microscope by first focusing on the specimen's surface and then on to the crack tip, at locations a and b, respectively. Multipling the difference in focus by the optical index of refraction for polystyrene (1.64) yields the depth of the crack. The acoustic and optical depth values in Table I are in good agreement, i.e. the difference is smaller than 5%.

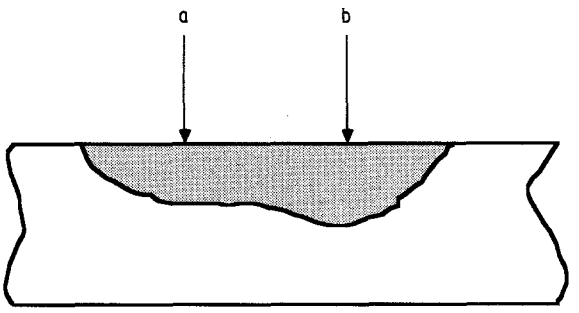

Figure 5 Geometry of crack 1 in polystyrene with scan positions a and b marked.

TABLE I Comparison between the crack depths determined from the $s(t, y)$ images in Fig. 4b and c and the direct optical measurements with a light microscope at locations a and b.

	Crack depth (μm)	
Method	*a*	*b*
Optical	52	70
Acoustic	50	73

A second example is given in Fig. 6a. Fig. 6a shows an $s(t, y)$ image taken near the end of a long through-thickness crack (crack 2). There are two diffracted signals seen in the $s(t, y)$ image. The diffracted signal is from a kink 53 μm below the surface and the second is caused by the 76 μm deep crack tip. The first segment of the crack, running from the surface down to the kink at 53 μm, appears to be perpendicular, because the crossing point of the surface-wave reflection and the vertex of the hyperbola are at the same y position. The inclination of the remaining segment of the crack can be found from the shift $\Delta y = 9\ \mu m$ between the two diffracted signals as 69°. Although this second crack segment should presumably give rise to a reflection from the segment face, such as line e in Fig. 3, no corresponding signal can be observed in the $s(t, y)$ image. However, optical measurements show that the segment is actually curved in shape rather than straight, and this could account for the lack of the crack-face reflection. Fig. 6b shows a schematic cross-section through the crack, and a comparison between the acoustic and optical measurements is given in Table II. Again the agreement between the results is better than 95%.

In aluminium, the diffracted signals from the crack tip are not as easily observable in the original $s(t, y)$ image as they are in polystyrene. This difference is mainly a result of the much larger acoustic impedance of aluminium: less energy is transmitted into the material, so that the tip-diffracted signal is weaker, while more energy is reflected from the specimen surface, so that the specular signal is stronger. Furthermore, in both materials the tip-diffracted signal may be buried in the strong specular reflection if the crack is not deep enough. Thus it is often necessary to

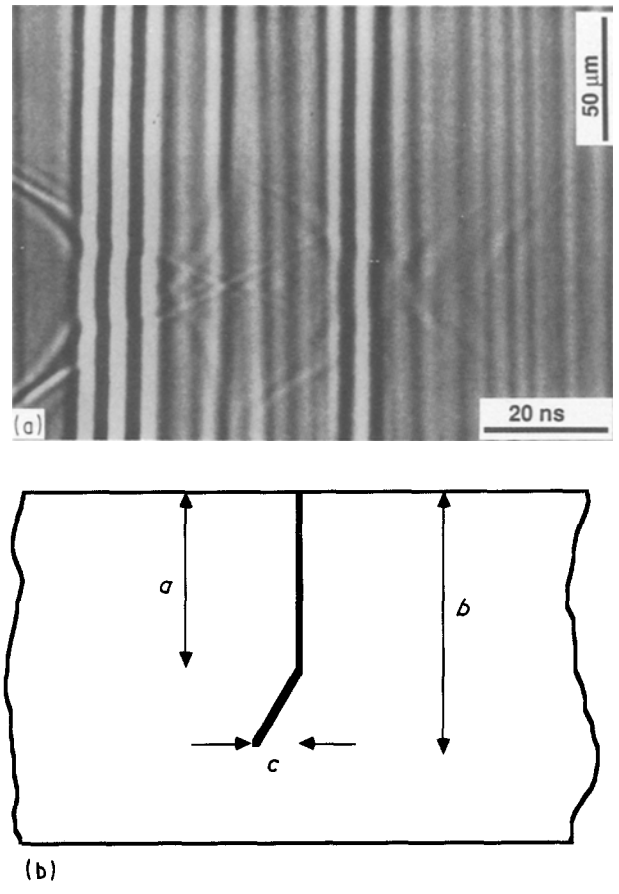

Figure 6 (a) An $s(t, y)$ image from crack 2 in polystyrene; $\Delta z = -60$ μm. The time range in the horizontal direction is 100 ns and the scan range in the vertical direction is 170 μm. (b) Geometry of crack 2 into the specimen at this location along the crack.

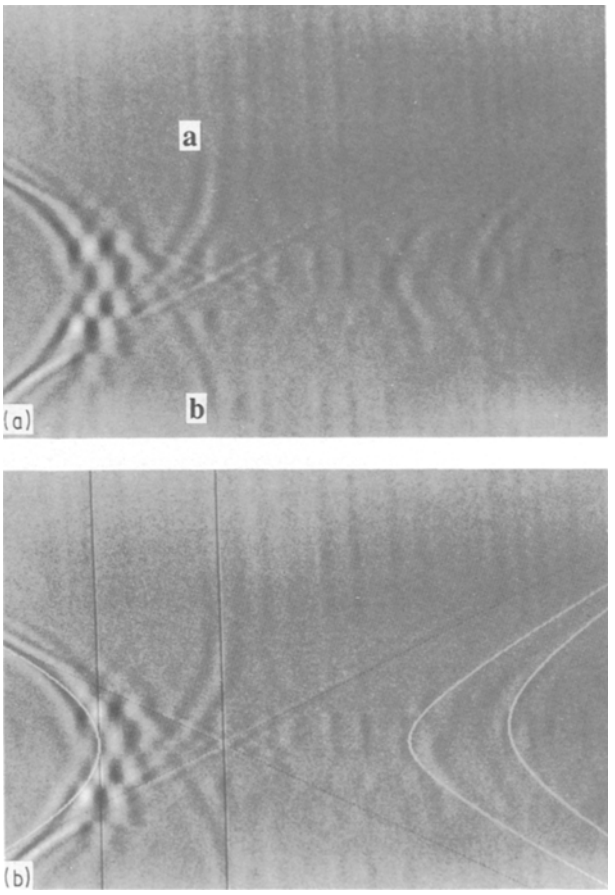

Figure 7 (a) The $s(t, y)$ image in Fig. 6a after the removal of the strong specular reflection and the surface-wave transmission signal. (b) Overlap between (a) and ray theory calculations.

TABLE II Comparison between optical and acoustic measurements of the depth of crack 2 (see Fig. 6b)

	Crack depth (μm)		
Method	*a*	*b*	*c*
Optical	52.5	75.5	10
Acoustic	54.5	72	9

use image processing in order to remove the specular reflection and to enhance the tip-diffracted signal contrast. As an example, Fig. 7a shows the $s(t, y)$ image of Fig. 6a after image processing. The image processing algorithm used is based on first aligning each time line in the $s(t, y)$ image with a reference line. This is done by interpolating the maximum in the cross-correlation between the two in order to find the necessary time shift, followed by an application of the appropriate time shift in the frequency domain (thus allowing for time shifts that are not integer values of the sample spacing, Δt). Then a scaled version of the reference line is subtracted from the original $s(t, y)$ time line to produce the processed line. The scale factor is determined by a least-squared-error fit between the reference and the original line. The reference line itself is determined as a moving average of the prior shifted original $s(t, y)$ time lines, thus allowing for some flexibility in handling slowly varying specular signals. At the same time a filter is applied in the frequency domain in order to remove the cable echo. The aligning and subtraction algorithm is designed to eliminate the signals which do not change as the lens is scanned, i.e. the specular and surface-wave transmission. Thus, in Fig. 7a the crack-mouth diffracted signal still appears after processing (hyperbola-shaped signal on the left of the $s(t, y)$ image). Furthermore, two additional lines (labelled a and b) appear in Fig. 7a that were not observable in the unprocessed image. They are caused by the scattering of surface waves at the crack mouth into rays in the fluid which then travel directly back to the lens. For lens locations sufficiently removed from the crack mouth these signals approach and meet the surface-wave transmission signal. Finally, the contrast of the tip-diffracted signals in the processed $s(t, y)$ image is considerably increased over that in the unprocessed image, and the time distances between their vertex points and the crossing point of the surface-wave reflections can be measured more precisely. An overlap between the $s(t, y)$ image of Fig. 7a and the signal time-of-fight traces calculated by ray theory, and based on the crack geometry in Fig. 6b, is given in Fig. 7b. The ray theory is based on calculating the travel time for pulses propagating along the appropriate ray paths, as shown in Fig. 2. For example, the time of arrival, T, for the specular reflection is given by $T = 2(F - \Delta z)/c_w$, where Δz and c_w are as before, and F is the lens focal length.

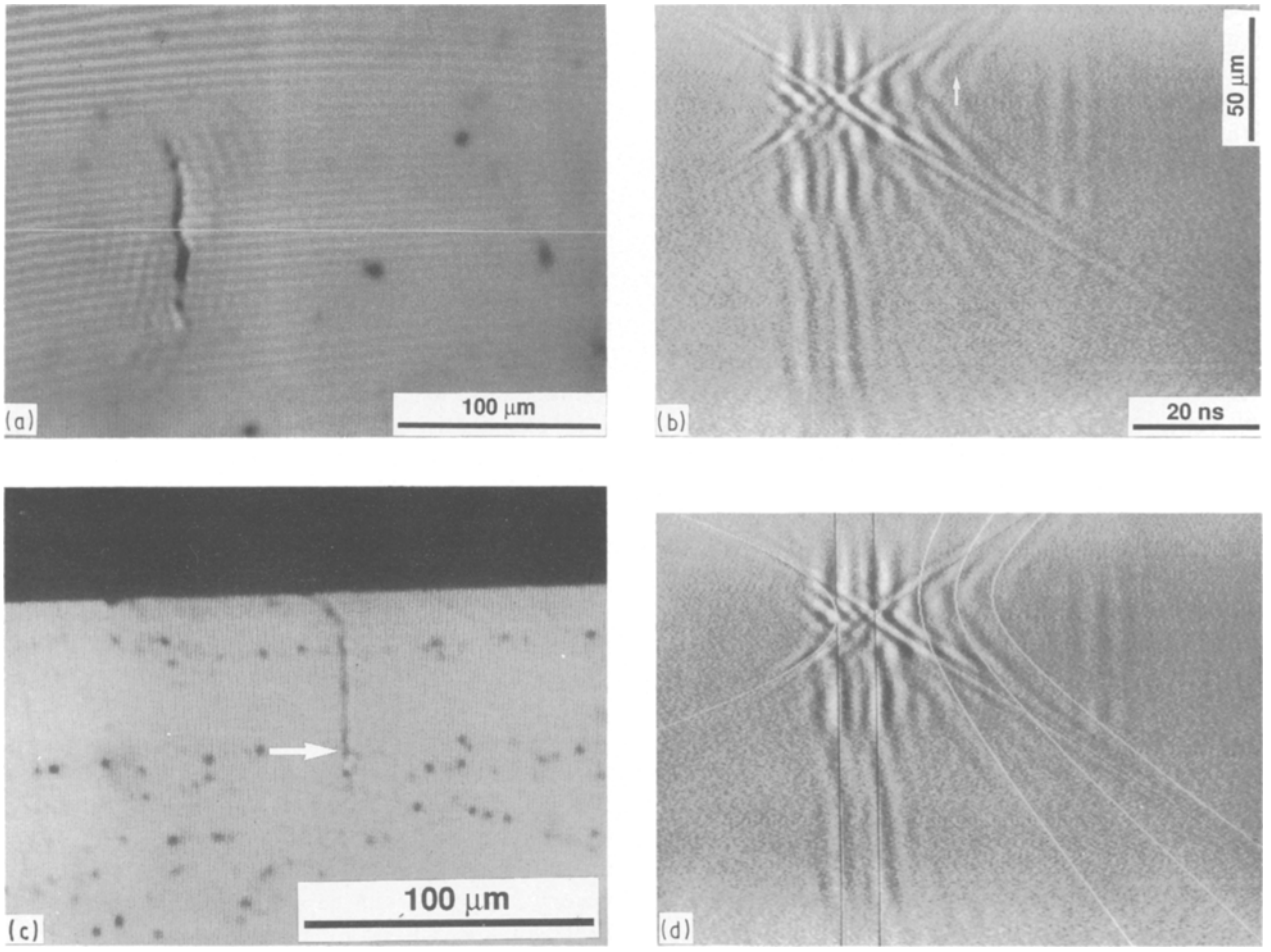

Figure 8 (a) Acoustic micrograph of a fatigue crack in Al–Li alloy 8090; $\nu = 350$ MHz and $\Delta z = 0$ μm. (b) The $s(t, y)$ image along the indicated line in Fig. 8a after processing; $\Delta z = -40$ μm. The time range in the horizontal direction is 100 ns and the scan range in the vertical direction is 185 μm. (c) Acoustic micrograph showing a cross-section of the crack; $\nu = 500$ MHz and $\Delta z = 0$ μm. The depth of the crack is 43 μm. (d) Overlap between (b) and ray theory calculations.

An acoustic micrograph of a fatigue crack in Al–Li alloy 8090 is shown in Fig. 8a taken at a frequency of 350 MHz and zero defocus. Unlike cracks in polystyrene, which are typically straight along the surface with a simple geometry into the specimen, cracks in aluminium have a more irregular shape both along the surface and into the specimen. Fig. 8b shows the $s(t, y)$ image taken along the scanning line indicated in Fig. 8a after image processing. In the unprocessed $s(t, y)$ image the specular and surface-wave transmission signals appeared essentially as in the $s(t, y)$ images of cracks in polystyrene and so the processing algorithm works to eliminate them as before. However, whereas the acoustic waves in water couple well only to longitudinal waves in polystyrene, both longitudinal and shear waves are excited by the SAM in aluminium. Thus, in aluminium there are longitudinal, shear and mode-converted signals created by diffraction at the crack tip, and this complicates the evaluation of the processed $s(t, y)$ image. The increased difficulty in interpreting the image is evident in Fig. 8b. The shear-wave tip-diffracted signal, though, has the longest travel time of the three, and also has a wave speed very close to the Rayleigh wave velocity. This means that the shear-wave signal will appear last (furthest from the surface-wave reflection crossing point), and will remain inside the surface-wave reflections for most of the hyperbola-shaped signal, and will have asymptotic slopes close to those of the surface-wave reflections. Thus the vertex of the shear-wave tip-diffracted signal has been identified, as marked in Fig. 8b. The depth of the crack obtained from the time distance measured between the crossing point of the surface-wave reflection and the shear-wave tip-diffracted vertex, plus the calculated time between crossing point and specular reflection, is 42 μm. Furthermore, the vertex of this tip-diffracted signal is shifted by 7 μm in the y direction, which means that the tip of the crack is shifted by 7 μm from directly below the mouth of the crack.

To confirm the acoustic depth determination the specimen was cut in order to provide a cross-section through the crack for examination. Fig. 8c shows an acoustic micrograph of the cross-section taken at 550 MHz and $\Delta z = 0$ μm. From this micrograph a crack depth of 43 μm is obtained and a shift between the crack tip and mouth of 6.5 μm, indicated by an arrow in Fig. 8c, is found. There is also an 8 μm deep kink visible which could not be determined from the $s(t, y)$ image in Fig. 8b. Even with the image processing this kink is unfortunately not deep enough and thus any signals from it remain buried by the strong specular and surface-wave signals.

An overlap is given in Fig. 8d between the experi-

mental, processed $s(t, y)$ image and the signal time-of-flight traces calculated by ray theory, and based on the crack geometry in Fig. 8d. The agreement between them is fair, and remaining differences could be due to errors in the wave speeds and the position of the cross-section through the crack, which may be slightly different from the position of the acoustic scan. Wave speeds in 8090 Al–Li alloy calculated from the elastic constants given by Müller *et al.* [14] are: $c_L = 6.8\ \mu m\ ns^{-1}$, $c_S = 3.6\ \mu m\ ns^{-1}$, and $c_R = 3.4\ \mu m\ ns^{-1}$. The density of Al–Li alloy 8090 is $\rho = 2.46\ g\ cm^{-2}$. The three approximately hyperbola-shaped white lines in Fig. 8d are the calculated time-of-flight traces for tip-diffracted longitudinal (first), mode-converted (middle) and shear waves (last). The mode-converted signal contains ray paths to and from the crack tip of different wave types. For example, if the incident ray is longitudinal, then the mode-converted diffracted ray will be transverse. Signals diffracted from the kink and waves reflected from the face of the inclined part of the crack are not directly visible in the $s(t, y)$ image of Fig. 8b.

4. Discussion

The present results demonstrate the capability of the acoustic microscope to determine the depth of short cracks in the transparent polymer polystyrene and in the Al–Li alloy 8090. Because of the small amplitude of the tip-diffracted signals it is necessary to use signal averaging in order to increase the signal-to-noise ratio. Even so the presence of the strong specular and surface-wave transmission signals in the original $s(t, y)$ images results in a relatively weak contrast for the tip-diffracted signals, so that appropriate image processing is necessary in order to remove these strong signals and further enhance the tip-diffracted signal contrast. Compared with polystyrene, cracks in metals propagate with a more irregular shape, and the SAM couples to both longitudinal and shear waves in the material, resulting in a considerably more complex $s(t, y)$ image. All of this complicates the recognition of tip-diffracted signals and the measurement of the vertex location. Further image processing, such as the application of a SAFT algorithm [15] based on the ray theory time-of-flight calculations, could possibly be used to improve the contrast and help to identify the signals. In addition, the shape of the tip-diffracted signals in metals depends in general on the degree and nature of the anisotropy of the material. Al–Li alloy 8090 has a very low anisotropy factor [14] and was considered to be isotropic for this work. Certainly the interpretation of the $s(t, y)$ images from more anisotropic materials will be more demanding.

Another aspect in the determination of crack depth with acoustic waves in metals is crack closure, caused by the plastic zone at the crack tip [16–18]. If the crack is closed near the tip then only diffracted signals from the end of the open segment may occur and the crack depth determined from the acoustic measurements will be too small. Therefore, it may be necessary to strain the specimen during the acoustic depth measurements in order to open the crack completely and measure the correct depth. If the crack is completely open, the applied stress corresponds to the crack closure stress. Thus TOFD also offers the potential to measure crack closure stresses.

5. Conclusions

The present investigations of short cracks measurements with the acoustic microscope and the TOFD technique have demonstrated the capability of the combination to detect and size cracks. The results obtained from the work could be summarized as follows:

1. The agreement between acoustic and optical depth determination in polystyrene is better than 95%.
2. The approach is not limited to "ideal" materials such as polystyrene but is also useful for metals such as the aluminium alloys.

The effects of crack closure and the anisotropy of the material need to be investigated if the approach is to be extended to other metals.

Acknowledgements

This project was funded through a grant from SERC and National Power, Grant no. GR/E 76391. We thank Dr A. Camyab and Dr I. Milne, National Power, for advice and support, and are grateful to Professor J. Kushibiki for providing the lens used in these studies. We also thank Professor Sir P. B. Hirsch who provided the laboratory facilities, and R. B. Thompson for the initial ray-timing work and continued support.

References

1. D. J. NICHOLLS and J. W. MARTIN, *Int J. Fatigue* **12** (1990) 469.
2. J. P. CHARLESWORTH and J. A. G. TEMPLE, "Ultrasonic Time-of-Flight Diffraction" (Wiley, 1989).
3. M. R. WEAVER, C. M. W. DAFT and G. A. D. BRIGGS, *IEEE Trans. Ultrason. Ferroelect. Frequency Control* **36** (5) (1989).
4. T. ZHAI, "Depth Measurements of Short Cracks in Perspex With The Scanning Acoustic Microscope", 20th International Symposium on Acoustical Imaging, Nanjing, China, 12–14 September, 1992.
5. M. G. SILK, *Ultrasonics* **17** (3) (1979).
6. J. A. OGILVY and J. A. G. TEMPLE, *ibid.* **21** (6) (1983).
7. G. A. D. BRIGGS, P. J. JENKINS and M. HOPPE, *J. Microscopy* **159** (1990) 15.
8. M. G. SOMEKH, in "Elastic Waves and Ultrasonic Nondestructive Evaluation", edited by S. K. Datta, J. D. Achenbach and Y. S. Rajapakse (1990).
9. M. G. SOMEKH, H. L. BERTONI, G. A. D. BRIGGS and N. J. BURTON, *Proc. R. Soc. Lond. A* **401** (1985) 29.
10. G. A. D. BRIGGS, "Acoustic Microscopy" (Oxford University Press, 1992).
11. K. H. CHAN and H. L. BERTONI, *IEEE Trans. Ultrason. Ferroelect. Frequency Control* **38** (1) (1991).
12. H. L. BERTONI, *IEEE Trans. Sonics Ultrason.* **su-31** (2) (1984).
13. R. H. TEW, J. R. OCKENDON and G. A. D. BRIGGS, in "Recent Developments in Surface Acoustic Waves", edited by D. F. Parker and G. A. Margin (Springer, 1988) pp. 309–16.
14. W. MÜLLER, E. BUBECK and V. GEROLD, in "Aluminium–Lithium Alloys III", Proceedings of the 3rd

International Aluminium–Lithium Conference (Institute of Metals, London).
15. S. F. BURCH, *Ultrasonics* **25** (9) (1987).
16. B. LONDON, J. C. SHYNE and D. V. NELSON, in "The Behaviour of Short Fatigue Cracks", edited by K. J. Miller and E. R. de los Rios (Mechanical Engineering Publications, 1986).
17. R. B. THOMPSON, C. J. FIEDLER and O. BUCK, in "Nondestructive Measurements for Materials Property Determination", edited by C. O. Ruud and R. E. Green (Plenum Press, New York, 1984) pp. 161–70.
18. R. B. THOMPSON, B. J. SKILLINGS, L. W. ZACHARY, L. W. SCHMERR and O. BUCK, in "Review of Progress in Quantitative Nondestructive Evaluation", Vol. 12A, edited by D. O. Thompson and D. E. Chimenti (Plenum Press, New York, 1982) pp. 325–41.

Received 26 February
and accepted 29 September 1992